An Analysis of Error Inducing Parameters in Multihop Sensor Node Localization

Andreas Savvides, Wendy L. Garber, Randolph L. Moses, *Senior Member*, *IEEE*, and Mani B. Srivastava, *Senior Member*, *IEEE*

Abstract—Ad hoc localization of wireless sensor nodes is a fundamental problem in wireless sensor networks. Despite the recent proposals for the development of ad hoc localization algorithms, the fundamental behavior in systems using measurements has not been characterized. In this paper, we take a first step toward such a characterization by examining the behavior of error inducing parameters in multihop localization systems in an algorithm independent manner. We first derive the Cramé Rao Bound for Gaussian measurement error for multihop localization systems using distance and angular measurements. Later on, we use these bounds on a carefully controlled set of scenarios to study the trends in the error induced by the measurement technology accuracy, network density, beacon node concentration, and beacon uncertainty. By exposing these trends, the goal of this paper is to develop a fundamental understanding of the error behavior that can provide a set of guidelines to be considered during the design and deployment of multihop localization systems.

Index Terms—Multihop node localization, sensor networks, Cramé Rao bounds, position estimation.

1 Introduction

Node localization in multihop sensor networks is a fundamental component of network self-configuration. When endowed with the ability to "sense" their location in space, ad hoc deployed sensor nodes can support a rich set of geographically aware protocols, and can accurately report the positions of detected targets or events.

One problem setup that received considerable attention in the literature is the case where a small fraction of the nodes in a multihop network are aware of their locations and act as *beacons* assisting other nodes to estimate their locations [1], [2], [3], [4], [5], [6]. Nodes with unknown locations use advertised beacon node locations and a set of distance or angular measurements to their neighboring nodes to estimate their locations. Despite their encouraging results, the proposed solutions do not provide a systematic decomposition of the resulting error in position estimates. Even in idealized setups with no obstacles or other external factors, relatively small error from noisy sensor measurements can induce much larger errors in node position estimates. This error is associated with a set of attributes that we refer to as the *network setup attributes*. The network setup attributes include the type of measurement technology used (distance or angle measurement), the accuracy of the measurement technology used, network density, uncertainties in beacon node locations, and beacon node densities.

In this paper, we examine localization error behavior with respect to the aforementioned network setup attributes. Our study considers the "idealized" case where measurements are not impacted by changes in the surrounding environment, and the underlying measurement error distribution is known. Under this assumption, we consider the error characteristics of different measurement technologies and a set of carefully controlled deployment setups, to develop a fundamental understanding of how network setup parameters affect the error behavior in node position estimates in systems that use distance and/or angular measurements. This study reveals a set of *guidelines* for the multihop localization problem. The resulting rules expose the trends associated with each of the network setup attributes and provides valuable insight into understanding the fundamental error behavior in multihop localization. Such knowledge can help to answer questions regarding the scalability of multihop localization, and provides a set of directions to consider as part the design cycle and during deployment. In addition to the preliminary results of our earlier work presented in [19], this paper provides the details of the bound derivations and includes a comparison of the error trade offs associated with the use of angular or distance measurements for localization. Moreover, it considers a wider range of scenarios, and provides some indication of how beacon location errors affect the final location estimates. To the best of our knowledge this is the first effort that constructs an analytical framework that attempts to characterize the trends error behavior for multihop localization.

Our analysis is based on analytical bounds for the covariance of localization parameter estimates, given by the Cramé-Rao bound for the case in which there is no beacon uncertainty, and the covariance bound on the maximum a

- *A. Savvides is with the Electrical Engineering Department, Yale University, 52 Prospect St # 212, New Haven, CT 06520. E-mail: andreas.savvides@yale.edu.*
- *W.L. Garber is with the ATK Mission Research Corporation, 3975 Research Blvd., Dayton, OH 45430-2108. E-mail: wendy.garber@atk.com.*
- *R.L. Moses is with the Department of Electrical and Computer Engineering, The Ohio State University, 2015 Neil Avenue, Columbus, OH 43210. E-mail: moses.2@osu.edu.*
- *M.B. Srivastava is with the Electrical Engineering Department, University of California, Los Angeles, 7702-B Boelter Hall, Box 951594, Los Angeles, CA 90095-1594. E-mail: mbs@ee.ucla.edu.*

Manuscript received 14 Nov. 2003; revised 29 June 2004; accepted 30 June 2004; published online 28 Sept. 2005.
For information on obtaining reprints of this article, please send e-mail to: tmc@computer.org, and reference IEEECS Log Number tmc-0192-1103.

TABLE 1
Expected Accuracy of Different Measurement Technologies

Technology	System	Measurement Accuracy (Intrinsic)	Range
Ultrasound	AHLoS	2cm	3m
Ultra Wide Band	PAL UWB	1.5m	N/A
RF Time of Flight	Bluesoft	0.5 m	100m
Laser Time of Flight	Laser range finder	1cm	75m

posteriori (MAP) estimate when beacon location uncertainty. These bounds provide an *analytical* means of characterizing localization uncertainty, thus avoiding Monte-Carlo simulations. On the other hand, the bounds are tight in the sense that maximum likelihood (ML) or MAP estimates of location parameters achieve these variance bounds for high signal-to-noise ratio.

This paper is organized as follows: The next section presents a classification of the error components and defines the problem. Section 3 presents the Cramé-Rao bound result for the multihop case. Section 4 describes our scenario setup and the simulation results. These results are summarized in Section 5.

2 Overview

2.1 A Classification of Error Components

Sensor measurement error can be broken down into two main categories, *extrinsic* and *intrinsic*. Extrinsic error is attributed to the physical effects on the measurement channel, such as the presence of obstacles, multipath and shadowing effects, and changes in the signal propagation speed due to changes in the surrounding environment. Intrinsic error is caused by imperfections of the sensor hardware and software. While extrinsic error is more unpredictable and harder to handle in realistic deployments, intrinsic error can also cause many complications when estimating node positions that utilize measurement information over multiple hops. Even relatively small measurement errors can significantly amplify the error in position estimates. This error amplification is inherently related to the network setup parameters. Denser deployment, for example, increases the number of possible measurements and, thus, helps to reduce the error in position estimates. Other changes such as the use of a lower precision measurement technology and higher uncertainty of beacon locations will induce increased errors in position estimates.

In this paper, we consider a range of intrinsic error characteristics representative of different measurement technologies. Table 1 lists the typical intrinsic average measurement error of four different systems: the ultrasonic distance measurement system used in the AHLOS project [4], ultra-wide-band system [7], RF Time-of-Flight system [8], and a SICK laser range finder [9]. With the trends exposed in this paper, one should be able to answer a set of fundamental questions regarding the use of each technology. Examples of such questions are listed below:

- What deployment density is required to achieve a certain localization accuracy with a particular technology?
- What are the trade offs between the use of distance versus angular measurements?
- Is the use of measurements over multiple hops scalable? How does error propagate?
- How does beacon density improve localization accuracy?
- How does beacon uncertainty affect the node position estimates?

2.2 Problem Statement

Assume we have a set of N sensors in a plane, with unknown locations $\{r_i = (x_i, y_i)\}_{i=1}^{N}$ and unknown orientation angles $\{\theta_i\}_{i=1}^{N}$. The orientation angles can be thought of as rotation angles of the sensor nodes' local frame of reference with respect to an absolute reference frame. In addition, a set of B beacon with locations $\{r_i = (x_i, y_i)\}_{i=-B+1}^{0}$ and orientations $\{\theta_i\}_{i=-B+1}^{0}$ are placed in the plane. The beacon locations and orientations are assumed to be known, but perhaps with some uncertainty. We define the location parameter vectors

$$\alpha_B = [x_{-B+1}, y_{-B+1}, \theta_{-B+1}, \ldots, x_0, y_0, \theta_0]^T \qquad (3B \times 1), \quad (1)$$

$$\alpha_N = [x_1, y_1, \theta_1, x_2, y_2, \theta_2, \ldots, x_N, y_N, \theta_N]^T \qquad (3N \times 1), \quad (2)$$

$$\alpha = \begin{bmatrix} \alpha_B \\ \alpha_N \end{bmatrix} \qquad (3(B+N) \times 1), \quad (3)$$

where α_B contains beacon node location parameters and α_N contains unknown (nonbeacon) node location parameters. Each beacon node advertises its location and orientation and this information is forwarded to the other nodes in the network.

For node localization, each sensor node and beacon node emits a known signal that allows neighboring nodes to estimate their distance and/or angle to the emitting node.

The measurements contain measurement error. We denote the distance measurement at node i to node j as $\hat{d}_{ij}$

$$\hat{d}_{ij} = d_{ij} + e_{d_{ij}}, \quad (4)$$

$$d_{ij} = \|r_i - r_j\| = \sqrt{(x_i - x_j)^2 + (y_i - y_j)^2}, \quad (5)$$

where $e_{d_{ij}}$ is the distance measurement error and where d_{ij} is the true distance between nodes i and j. We denote the angle measurement at node i to node j as $\hat{\phi}_{ij}$

$$\hat{\phi}_{ij} = \phi_{ij} + e_{\phi_{ij}}, \tag{6}$$

$$\phi_{ij} = \theta_i + \angle(r_i, r_j) = \theta_i + \tan^{-1}\left(\frac{y_i - y_j}{x_i - x_j}\right), \tag{7}$$

where $e_{\phi_{ij}}$ is the angle measurement error and where ϕ_{ij} is the true angle between nodes i and j, measured with respect to node i's *local* frame of reference.

We will consider four localization subproblems. First, the nodes may or may not measure angles to emitting nodes. This may be the case for sensor nodes having a single, omnidirectional sensor. In this case, orientations of sensors are not identifiable, and the θ_i elements are removed from the α_B and α_N vectors, and their dimensions reduce to $(2B \times 1)$ and $(2N \times 1)$, respectively. If angle measurements only or if distance and angle measurements are collected, the localization solution includes both position and orientation estimates of sensor nodes. Second, the beacon node locations (and orientations) are either assumed to be known exactly, or assumed to have uncertainty. When they have uncertainty, we simultaneously estimate both sensor node and beacon node locations (and orientations), as the measurements provide additional information about beacon locations (and orientations) that reduce the uncertainty.

We denote the availability of a measurement from node i from a signal emitted at node j (for $i, j = -B+1, \ldots, N$) using the indicator function I_{ij}, where $I_{ij} = 1$ if the signal is detected and $I_{ij} = 0$ otherwise. Depending on the particular subproblem being considered, $I_{ij} = 1$ indicates that a distance measurement, an angle measurement, or both measurements are observed. The measurement are stacked into a vector X whose length is defined to be M.

In this paper, we assume the measurement errors are independent Gaussian random variables with zero mean and known variances σ_d^2 and σ_ϕ^2, respectively. We acknowledge that although this uncorrelated-Gaussian measurement error does not capture all practical cases, it is a good starting point for exposing some of the error trends in multihop networks. More general cases are considered in [10], [11].

The general localization problem statement is as follows: Given noisy distance measurements $\hat{d}_{ij}$ and/or noisy angle measurements $\hat{\phi}_{ij}$, beacon locations r_i, and orientations θ_i for $i = -B+1, \ldots, 0$, estimate the locations $\hat{r}_i$ and orientations $\hat{\theta}_i$ for $i = 1, \ldots, N$. We note that the orientations $\hat{\theta}_i$ are only estimated when angle measurements are available.

3 Localization Error

In this section, we develop two analytical expressions for sensor node localization error. The first assumes beacon nodes have known locations and orientations. In this case, the localization accuracy is computed using the the Cramér Rao bound (CRB) [10]. When beacon nodes have location uncertainty, we characterize localization accuracy using a covariance bound that is similar to the CRB. Both bounds are tight in the sense that localization algorithms (specifically, maximum likelihood parameter estimates in the known-beacon case and maximum a posteriori parameter estimates in the uncertain-beacon case) achieve these bounds for high measurement signal-to-noise ratio. In addition, the bounds are computed analytically, and avoid the need for expensive Monte-Carlo simulations. The computational advantage afforded by analytical bounds permit us to study localization performance for a large number of network topologies.

3.1 Localization Error Bound for Multihop Topologies with Known Beacon Locations

When beacon nodes have known location (and, if applicable, orientation), the CRB is used to bound localization error. The CRB gives a lower bound on the error covariance matrix for an unbiased estimate of parameter vector α_N (see, e.g., [12]). The lower bound is given in terms of the Fisher Information Matrix $J(\alpha_N)$. Let $\hat{\boldsymbol{\alpha}}_N$ be any unbiased estimate of parameter α_N based on observation vector X having a pdf of $f_X(x)$. The error covariance matrix is defined as

$$C = E\{(\hat{\boldsymbol{\alpha}}_N - \alpha_N)(\hat{\boldsymbol{\alpha}}_N - \alpha_N)^T\}. \tag{8}$$

This error covariance matrix is bounded below by the CR bound, which is given by

$$CRB = [J(\alpha_N)]^{-1}, \tag{9}$$

where the matrix $J(\alpha_N)$ is given by

$$J(\alpha_N) = E\Big\{[\nabla_{\alpha_N} \ln f_X(X;\alpha_N)][\nabla_{\alpha_N} \ln f_X(X;\alpha_N)]^T\Big\}. \tag{10}$$

The matrix $J(\alpha_N)$ is called the Fisher Information Matrix (FIM).

The $(M \times 1)$ measurement vector X in (10) is a vector formed by stacking the available distance measurements $\hat{d}_{ij}$ and/or the angle measurements $\hat{\phi}_{ij}$, where the (ij) pairs correspond to those for which $I_{ij} = 1$. Thus, the mth element of X has a corresponding value of i and j. Since it is assumed that the measurements are Gaussian, the measurement pdf is the vector Gaussian pdf

$$\begin{aligned} f_X(x;\alpha_N) &= \mathcal{N}(\mu(\alpha_N), \Sigma) \\ &= \frac{1}{(2\pi)^M |\Sigma|^{\frac{1}{2}}} \exp\left\{-\frac{1}{2}[x-\mu(\alpha_N)]^T \Sigma^{-1} [x-\mu(\alpha_N)]\right\}, \end{aligned} \tag{11}$$

where the mean vector $\mu(\alpha_N)$ is a vector of true distances and angles whose elements are given by (5) and (7) and are stacked in the same order as the measurements in X. When the measurements are uncorrelated, the covariance matrix Σ in (11) is diagonal, and the diagonal elements Σ_{kk} are σ_d^2 for distance measurements and σ_ϕ^2 for angle measurements. However, the derivation that follows holds for more general Σ matrices.

For the measurement pdf in (11), we find that

$$J(\alpha_N) = [G'(\alpha_N)]^T \Sigma^{-1} [G'(\alpha_N)], \tag{12}$$

$$[G'(\alpha_N)]_{m,n} = \partial \mu_m(\alpha_N) / \partial \alpha_{Nn} \qquad (M \times \dim(\alpha_N)). \tag{13}$$

The partial derivatives in (13) are readily computed from (5) and (7), (2), and (11).

The mth element $\mu_m(\alpha_N)$ is either a distance d_{ij} or an angle ϕ_{ij} for some corresponding i and j; thus, for each $m \in [1, M]$ there is a corresponding pair (i, j), and we denote this correspondence as $m \leftrightarrow (i, j)$. Similarly, the nth element of α_N, denoted α_{Nn} is one of $\{x_{i'}, y_{i'}, \theta_{i'}\}$ for some

corresponding $i' \in [1, N]$ and we denote the correspondence $\alpha_{Nn} \leftrightarrow x_{i'}$ or $\alpha_{Nn} \leftrightarrow y_{i'}$ or $\alpha_{Nn} \leftrightarrow \theta_{i'}$. With this notation, if the mth element of $\mu(\alpha_N)$ is a distance d_{ij} with $m \leftrightarrow (i,j)$, then from (5) we have

$$[G'(\alpha_N)]_{mn} = \begin{cases} \frac{x_i - x_j}{d_{ij}}, & \alpha_{Nn} \leftrightarrow x_i \\ \frac{x_j - x_i}{d_{ij}}, & \alpha_{Nn} \leftrightarrow x_j \\ \frac{y_i - y_j}{d_{ij}}, & \alpha_{Nn} \leftrightarrow y_i \\ \frac{y_j - y_i}{d_{ij}}, & \alpha_{Nn} \leftrightarrow y_j \\ 0, & \text{otherwise.} \end{cases} \quad (14)$$

Similarly, if the mth element of $\mu(\alpha_N)$ is an angle, say ϕ_{ij} for some corresponding values of i and j, then from (7) we have

$$[G'(\alpha_N)]_{mn} = \begin{cases} \frac{y_j - y_i}{d_{ij}^2}, & \alpha_{Nn} \leftrightarrow x_i \\ \frac{y_i - y_j}{d_{ij}^2}, & \alpha_{Nn} \leftrightarrow x_j \\ \frac{x_i - x_j}{d_{ij}^2}, & \alpha_{Nn} \leftrightarrow y_i \\ \frac{x_j - x_i}{d_{ij}^2}, & \alpha_{Nn} \leftrightarrow y_j \\ 1, & \alpha_{Nn} \leftrightarrow \theta_i \\ 0, & \text{otherwise.} \end{cases} \quad (15)$$

The CRB is then given by the inverse of the FIM as in (9).

3.2 Localization Error Bound for Multihop Topologies with Uncertain Beacon Locations

When the beacon locations have some uncertainty, we model the beacon localization parameter vector α_B as a random vector with a (known) prior pdf $f_0(\alpha_B)$. We assume the prior pdf is Gaussian:

$$f_0(\alpha_B) \sim \mathcal{N}(\mu_0, \Sigma_0), \quad (16)$$

where μ_0 is the vector of nominal location (and orientation) of the beacon nodes and Σ_0 is the beacon location (and orientation) uncertainty. For the case of distance-only measurements, α_B contains only x_i and y_i parameters, and is of size $(2B \times 1)$.

When beacon locations are uncertain, the measurement vector X informs about node localization for both unknown nodes and beacon nodes. Thus, we can estimate the unknown sensor node locations (and orientations) and simultaneously estimate the beacon locations (and orientations), thereby reducing beacon uncertainty. We do so by estimating the combined parameter vector, α, in (3).

The pdf $f_0(\alpha_B)$ provides prior information about the parameter vector α_B, as given by

$$J_0 = E\Big\{[\nabla_\alpha \ln f_0(\alpha_B)][\nabla_\alpha \ln f_0(\alpha_B)]^T\Big\}.$$

For the Gaussian pdf assumed in (16), the corresponding information matrix is found to be:

$$J_0 = \begin{bmatrix} \Sigma_0^{-1} & 0 \\ 0 & 0 \end{bmatrix}. \quad (17)$$

We will assume in the numerical studies in Section 4 that Σ_0 is diagonal with elements $\sigma_{0,d}^2$ corresponding to location parameters and $\sigma_{0,\phi}^2$ corresponding to orientation parameters. However, (17) applies to more general prior errors. For example, if the x and y location errors for each beacon node are correlated, then Σ_0 is block-diagonal, with 2×2 block representing the covariance of the (x, y) errors for each node. In addition, if beacon locations are known (with some uncertainty) but there is no prior orientation information, then Σ_0^{-1} has zeros on the diagonal elements corresponding to the θ_i parameters.

The information provided by the measurements and the a priori information are assumed to be independent, and can be summed. Thus, the total information matrix is given by [12]:

$$J_T = J(\alpha) + J_0, \quad (18)$$

where $J(\alpha)$ is given by (12) with α_N replaced by α. Then, as with the CRB, a lower bound on the mean squared error C of an estimate of α is given by

$$C \geq J_T^{-1}. \quad (19)$$

The bound J_T^{-1} in (19) is used to study localization performance for multhop topologies when beacon nodes have uncertain location (and orientation).

4 Localization Performance Analysis

In this section, we analyze the localizaton properties of several multihop network topologies, using the covariance bounds derived in the previous section. Our goal is to characterize localization performance as a function of several sensor network characteristics, such as node density, percentage of beacon nodes, network size, and beacon uncertainty. To do so, we generate several network topologies that have similar characteristics (for example, similar node density), and compute the localization error bound using (9) or (19), depending on whether the beacon node locations are uncertain or not. We then average the performance over these network topologies.

4.1 Network Generation

In this section, we describe the procedure by which we generate candidate networks with different characteristics. We characterize a network of nodes by its density, total size, and node detection range. Let $\bar{n}$ denote the average number of neighbors per node, let D denote the density of the network in nodes m^2, and let R be the detection range of the sensors in meters. We have the following relation

$$\bar{n} + 1 = \pi R^2 D. \quad (20)$$

We note that $\bar{n}$ corresponds the average number of neighbors per node only for nodes on the interior of the network. Nodes near the edge of the network will have fewer neighbors. We define the density as the number of nodes per square meter. As the density increases, the connectivity increases because there are more nodes within detection range of each other. The density and connectivity are are also closely related to the detection range of the sensors. To expose the trends in our study, the scenarios are designed so that the density is uniform across the network.

In addition to closely controlling network density, the generated scenarios also aim to minimize the effects of geometry. Bad geometry can induce more errors that that would make it more difficult to isolate the error components of the network setup parameters under investigation. The effects of geometry on computed locations has been

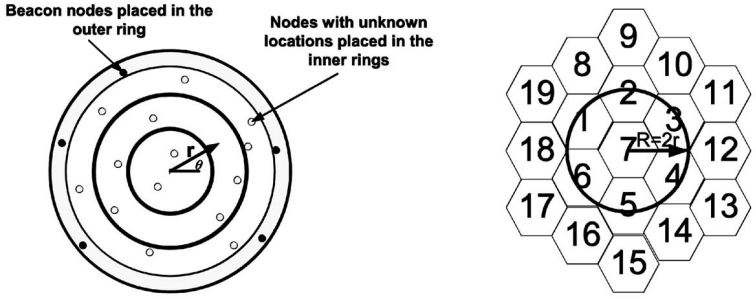

Fig. 1. Scenario generation (a) radial deployment pattern and (b) hexagon pattern, nodes outside the perimeter have exactly six neighbors each.

demonstrated as the geographic dilution of precision (GDOP) factor, described in previous work. A notable characterization of geometry error for the case where the locations of 1-hop anchor nodes is shown in (21) described in Spirito in [13].

$$GDOP = GDOP(N, \theta) = \sqrt{\frac{N}{\Sigma_i \Sigma_{j,j>i} |\sin(\theta_{ij})|^2}}. \quad (21)$$

N is the number of nodes used as anchors and θ_{ij} is the angle between each pair of nodes (i, j) used as anchor points by a node during the localization process. The relation in (21) shows that the error contribution due to unfavorable geometries is largest when the angles between two nodes acting as anchor points is very small or when the anchor points are across from each other, forming an angle close to 180 degrees.

To minimize the error associated with geometry, the scenarios are generated using a radial deployment pattern. Node positions are generated in polar coordinates by generating a radius r and an angle θ for each node. Nodes are deployed in a circular field, which is divided into a set of rings. The number of nodes deployed in each ring is proportional to the fraction of the area of the ring with respect to the total area of the circular field as shown in Fig. 1a. This pattern tries to approximate the effect of hexagonal cells (shown in Fig. 1b). In a hexagonal placement, a node is placed at the center of each hexagon and the detection range is set to R as shown in the figure. In this case, each node that is not part of the perimeter has exactly six evenly spaced (60° apart) neighbors. While this placement will isolate the geometry effects, it is only possible for hexagonal placement. The radial scheme described above aims to approximate this hexagonal placement for higher densities. Furthermore, to ensure that no nodes with unknown positions are placed on the boundaries, the beacon nodes are deployed in the outer ring of the circular sensor field. Varying the area of the field controls network density.

Fig. 2 shows three example networks having different densities, with beacons drawn as squares and unknowns drawn as circles. The networks in Figs. 2a and 2b were generated using the method described above. Both networks contain a total of 50 nodes, but the denser network occupies a smaller area and has more connections. These networks were generated assuming detection range of 10m. Circles in the figures denote node locations, and edges between nodes denote that they are within detection range of each other and, thus, that there is a distance and/or angle measurement between them that appears in the vector X. Fig. 2c is an example of a hexagonal deterministic deployment pattern used in some of the simulation experiments. In this network, all the nodes on the perimeter are beacon nodes, so each node with unknown location has exactly six evenly spaced neighbors.

4.2 Network Density

For this experiment, we generated a number of network scenarios with varying densities using the method described above. Each of these networks contain a total of 50 nodes, 10 of which are beacon nodes. The detection range was set to 10 m. For each density value examined, we compute the RMS location error for each of 20 different networks having the same density, using the computed CRB matrix associated with that network. From the CRB matrix, we compute the average RMS location error of each of the 40 nonbeacon nodes, computed as

$$\text{RMS error} = \frac{1}{40}\sqrt{\sum_{i=1}^{40}[CRB]_{(i-1)K+1,(i-1)K+1} + [CRB]_{(i-1)K+2,(i-1)K+2}}, \quad (22)$$

where $K = 2$ when α_N is $(2N \times 1)$ and $K = 3$ when α_N is $(3N \times 1)$. We then average this RMS error over the 20 networks, and compute the standard deviation of this RMS error for the 20 networks. We plot the average value as a function of network density, and we indicate the ± 1 standard deviation of this value with error bars on the figures.

The results using distance only measurements are shown in Fig. 3a, and results using angular measurements are shown in Fig. 3b. In these and all remaining figures, we have plotted the RMS location error (in meters) divided by the distance measurement standard deviation σ_d in meters (RMS error/σ_d), or by the angle measurement standard deviation σ_ϕ in radians (RMS error/σ_ϕ), which we write as (RMS error/σ) for short. By multiplying points on this curve by the measurement error that corresponds to a given sensor, the average location error is found. For example, the average RMS location error in a network with 20 neighbors/node

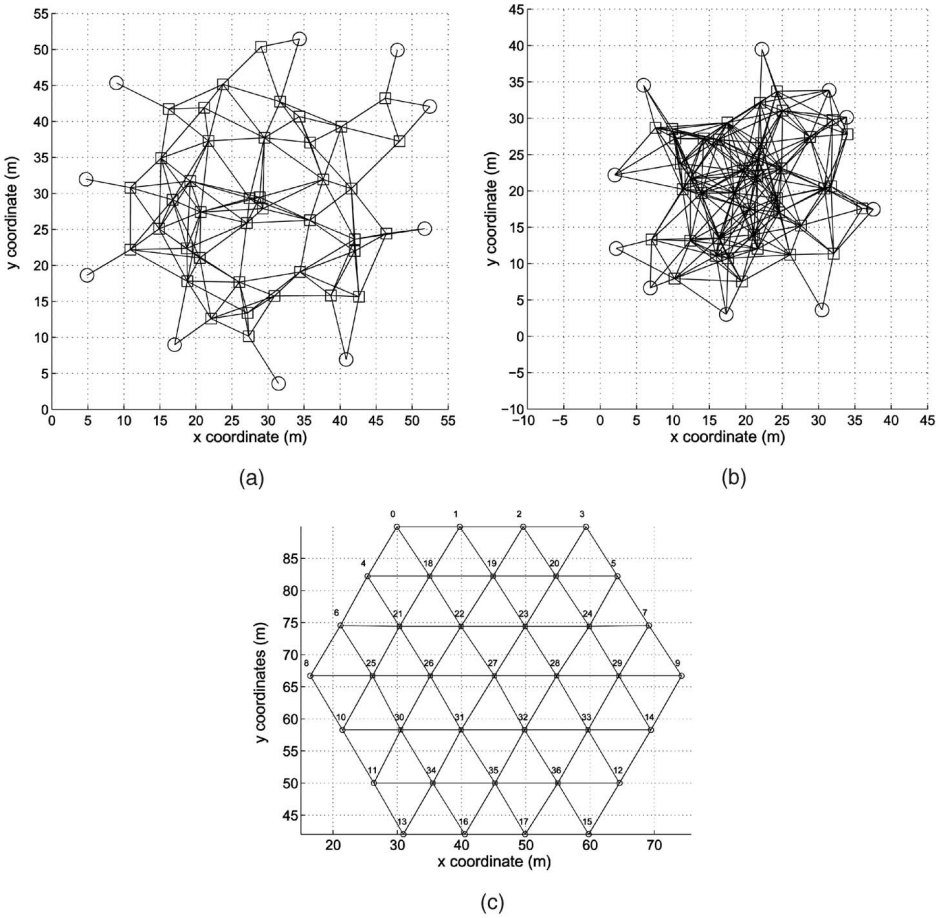

Fig. 2. Two example 50-node networks with different node densities. (a): 0.03 nodes/m^2; (b): 0.06 nodes/m^2. Circles are beacon nodes and squares are unknown nodes. Both networks have a detection range of 10 m, and edges in the graph correspond to node pairs for which distance or angle measurements are available: (c) A 37-node scenario where every unknown node has exactly six neighbors.

and a ranging technology with a 20 mm accuracy is given by $(0.02) \cdot (0.36) = 0.007$ m.

As we can see from these plots, the error does decrease with increasing connectivity for both distance and angular measurements. In the case of distance measurements, the decrease is rapid at first, then becomes more gradual. This suggests that after a certain point, increasing the density of the network may not be very beneficial to the localization process. We also note that the one standard deviation error bars are quite small.

Intuitively, one would expect an improvement in position estimates as the network density increases, due to the increase in measurement constraints. Both angular and distance measurements have an asymptotic response to density effects, where the effect of adding more neighbors in low density scenarios yields more improvement in position estimates. Furthermore, when angular measurements are used, density effect is also correlated to range, since the error contribution of angular measurements increases with distance.

The plot in Fig. 3b corresponds to angular measurements for the same set of scenarios as the one used to obtain the density trends when distance measurements are used in Fig. 3a. The two plots have similar shapes for a small number of node neighbors, but the RMS location error corresponding to angle measurements decreases more rapidly than for distance measurements when the number of neighbors becomes large. The primary source of this more rapid decrease is that when the node density increases, the average distance between nodes decreases, and the distance error corresponding to a fixed angular measurement error correspondingly decreases. Similarly, increasing the density by increasing the detection range, would increase the error in the angle measurement case. This is intuitive since the tangential error increases with range. Fig. 3c shows how the localization error behaves as the detection range is scaled for a 61-node hexagonal placement scenario. In the case of angle measurements, the localization error scales linearly with range, whereas for the case of distance measurements it remains constant. Fig. 3d shows a normalized version of the angle measurement trend that removes the effect of detection range. This plot was obtained by normalizing the node locations in each of the scenarios used with the average internode distance for the whole network. The trend in Fig. 3d is very similar to the distance only measurement trend in Fig. 3a.

From Figs. 3a and 3b, we can compare the distance and angle measurement accuracy requirements to achieve similar localization accuracy. At 10 neighbors/node and a distance measurement standard deviation of 20 mm, Fig. 3a

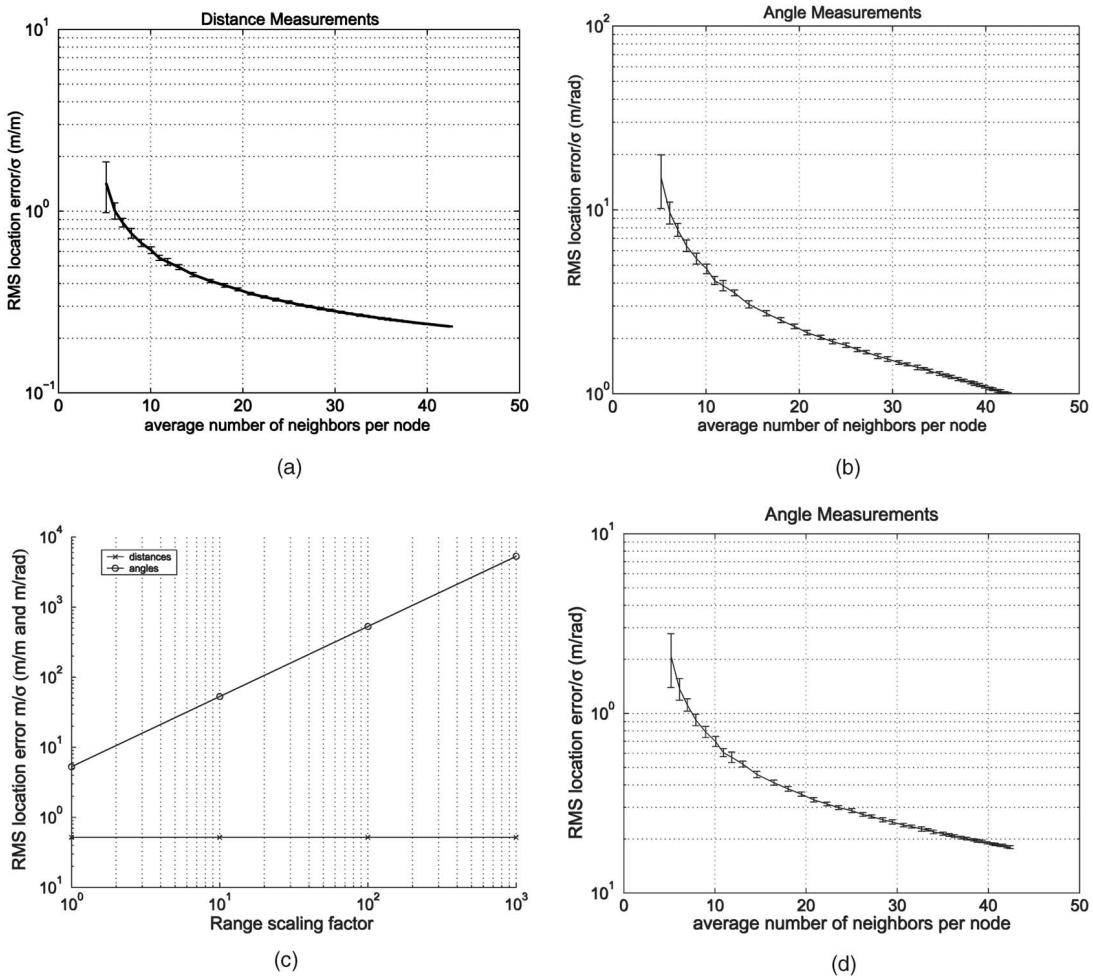

Fig. 3. Normalized RMS node localization error, (RMS error/σ) as a function of the average number of neighbors per node. (a) Using distance-only measurements with distance measurement error $\sigma = \sigma_d$. (b) Using angle-only measurements with angle measurement error $\sigma = \sigma_\phi$. (c) Localization error in hexagon scenario when internode range is scaled; the linear scaling of error for angle-only measurements corresponds to the linear dilation of tangential location error with range. (d) Angle-only localization error when node locations are normalized by the average distance between the nodes.

gives an average localization error of 0.012 m. From Fig. 3b, in order to achieve the same localization accuracy, one needs an angle measurement standard deviation of $\sigma_\phi = .012/4.8 = 0.0025$ rad, or $0.14°$. Even for very dense networks (each node having on average 42 neighbors), DOA measurements must be accurate to a standard deviation of $0.27°$ to achieve the same localization accuracy as that obtained using distance measurements with 20 mm standard deviation. This suggests that technologies using distance measurements such as acoustic ultrasonic and laser will produce higher accuracy locations than technologies using angle measurement only since very high precision measurements are required to achieve the same location accuracy as distance measurement technologies. The role of angular measurements, however, should not be overlooked. Recent work by Nicolescu and Nath in [14] have shown angle-only localization to produce favorable results.

4.3 Network Size

In this section, we investigate how the localization error varies as the network scales in overall size. We evaluate the CRB for a number of networks having a fixed density/connectivity (.03 nodes/m^2 or about eight neighbors per node), a fixed percentage of beacon nodes (10 percent of the nodes are beacons), and varying size. This means that we increase the area that the network occupies while increasing the number of nodes so as to keep the node density constant. Again, we compute the average RMS error/σ over 20 different networks having the same size and perform this experiment for both distance measurements and angle measurements. The results are shown in Fig. 4.

From Fig. 4, we can conclude that for both distance measurements and angle measurements the localization error is not greatly affected as the network scales. One might have expected that as a multihop network gets larger the nodes farther away from beacons might suffer from error propagation, thereby increasing the localization error. This is apparently not the case.

To further study the effect of the distance to beacon nodes on the localization error, we look at the RMS error at each node as a function of the number of hops to the nearest beacon node. Using 20 different networks, each containing 140 total nodes (of which 14 are beacon nodes), we compute the average RMS error as a function of the number of hops to the nearest beacon when distance measurements are

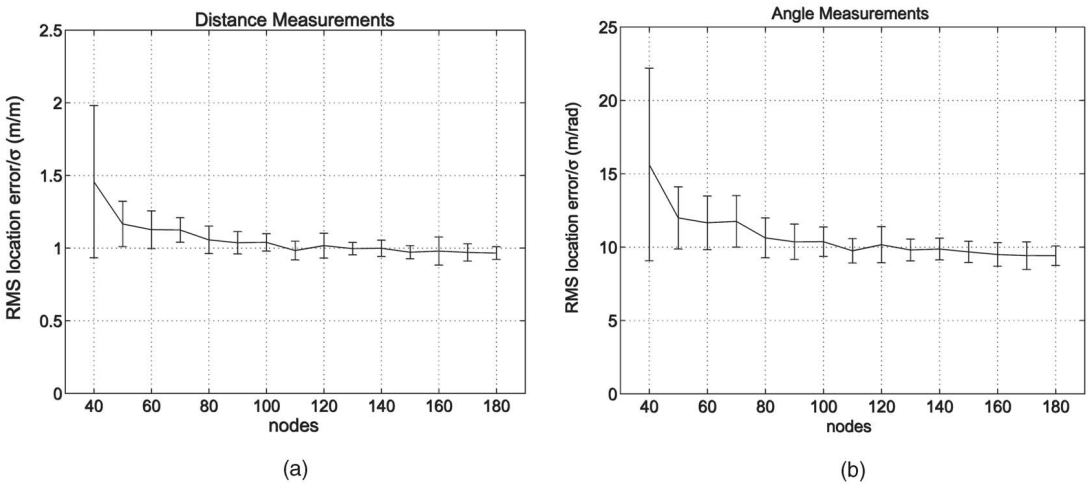

Fig. 4. Normalized RMS node localization error, (RMS error/σ) as a function of the number of nodes in the network. (a) Using distance-only measurements with distance measurement error $\sigma = \sigma_d$. (b) Using angle-only measurements with angle measurement error $\sigma = \sigma_\phi$.

used, and again when angle measurements are used. The results are plotted in Fig. 6. For the scenarios examined here, the localization error does not appear to vary greatly as the number of hops to the nearest beacon increases when distance measurements are used. Somewhat counterintuitively, the error appears to decrease as the distance to beacon nodes increases. We hypothesize that this decrease may be due to the fact that nodes far from a beacon are well in the interior of the network, and tend to have a slightly higher average number of neighbors than nodes close to a beacon; in addition, these neighbors are more likely to be in all directions, whereas nodes near beacons are also near boundaries, and tend to have fewer neighbors on one side than on the other. Initial results, reported in [15], support this hypothesis, but a more thorough study of this point is needed in order to make more concrete statements.

Fig. 5 shows how error propagates on a more controlled hexagonal deployment pattern with a total of 61 nodes, 24 of which are beacons. The plot on the left shows the profile of the error (magnified by a factor of 10) for the case where angle-only measurements are used. The plot on the left is a vertical cut-through that shows how the RMS location error increases for the nodes that are located toward the center of the hexagonal field. The error propagation increases sublinearly with the number of hops. The percentage increase in error from hop to hop is shown is shown in Table 2. The table shows that although the overall error is more when angle measurements are used, the hop-to-hop error propagation is slower when angle measurements are used.

4.4 Beacon Percentage

We next consider the effect of percent of beacon nodes on the localization error. In other words, we would like to find out if increasing the percentage of beacon nodes in the network improves the location estimates. To do this, we used a set of network scenarios, each having 100 total nodes. The number of beacons was varied from 4 to 20. The network density was held constant at 0.035 nodes/m^2 or about 10 neighbors per node. We again average the RMS error/σ for 20 different networks having the same beacon percentage to obtain each point on the curve. Fig. 7 shows

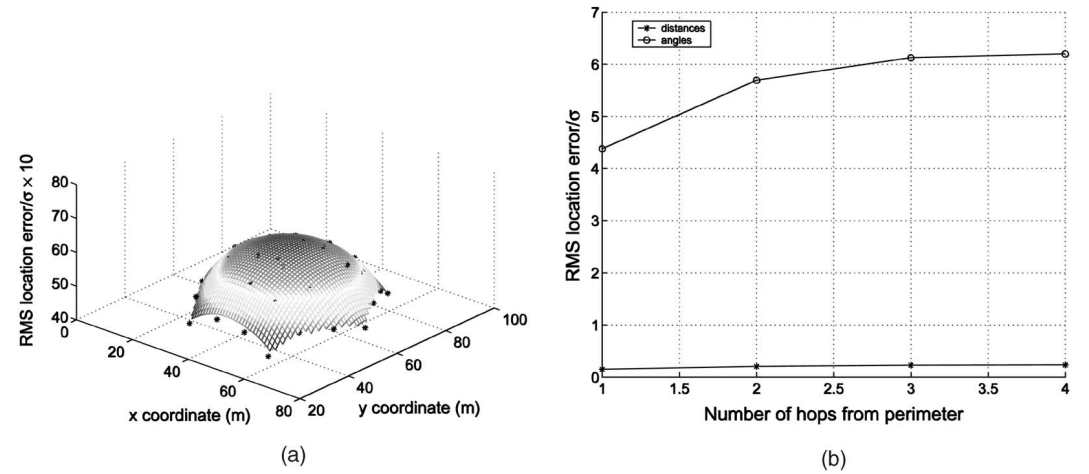

Fig. 5. RMS node localization error, (RMS for a 61-node hexagonal placement scenario). (a) Error profile when angle-only measurements are used. (b) Error propagation as the number of hops from the network perimeter increases.

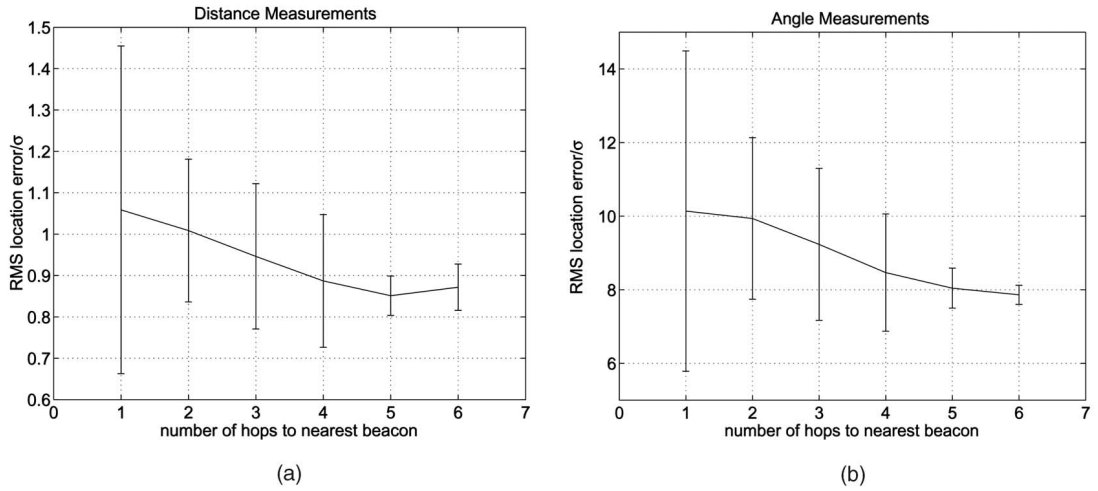

Fig. 6. Normalized RMS node localization error, (RMS error/σ) as a function of the number of hops to the nearest beacon node. (a) Using distance-only measurements, with distance measurement error $\sigma = \sigma_\phi$. (b) Using angle-only measurements with angle measurement error $\sigma = \sigma_\phi$.

the results of this experiment using distance and angle measurements. The percentage of beacons does not appear to have a large impact on the localization error.

4.5 Beacon Uncertainty

The beacon locations may not be known exactly, uncertainty in the beacon locations will affect the accuracy of the sensor location estimates. For this experiment, we have used the same network scenarios that were used in the network density experiment. Each network used contains 50 total nodes, 10 of which are beacons. We vary the relative beacon uncertainty standard deviation (σ_0/σ) from 0 to 3. The CRB matrix is computed using the method of Section 3.2 and the RMS error/σ is computed for nonbeacon nodes only. The results are averaged over 20 different network scenarios having the same density and for each density, we plot a curve showing the RMS error/σ as a function of the beacon uncertainty variance.

The resulting curves for distance measurements are shown in Fig. 8. At low σ_0, the localization error is dominated by the distance measurement error, but at higher σ_0 ($\sigma_0/\sigma > 1$), the localization error is dominated by σ_0 and increases linearly.

For higher beacon uncertainty values, it turns out that the *relative* location error between sensors remains small (on the order of that predicted when $\sigma_0 = 0$) and most of the location uncertainty error can be attributed to an overall translation of beacons from their nominal locations. More details on this aspect, and a derivation of the relative location error CRB, are found in [16].

TABLE 2
Percentage Increase in RMS Location Error with Hop Distance

	Hop 2	Hop 3	Hop 4
Distance measurements	36.75%	11.16 %	2.65%
Angle measurements	30%	7.61%	1.2%

5 Related Work

Some of the trends discussed here have been partially mentioned in works studying specific localization schemes. The quantitative comparison of different schemes presented in [17] and the references thereof, is a representative example of this effort. In [17] a detailed side-by-side comparison of three localization schemes is presented. This comparison gives some indications of the resulting localization error as observed from each of the three schemes considered. The drawback of using this approach in exposing the trends, is that some of the error introduced into the result is an artifact of the particular localization algorithm being used. Furthermore, the comparison in [17] considers a more limited set of scenarios that does not reveal all the trends and their association with the network setup parameters.

The most relevant work to this paper is the work presented in [18] and [6]. In [18], Patwari et al. use Cramé Rao bound analysis to analyze the performance of a localization system based on radio received signal strength. This study was more focused very specific scenarios. More recently, in [6], the Cramé Rao bounds for radio received signal strength and round-trip TOA of RF signals are considered; since RF signals were used, timing accuracies for TOA measurements on the order of 1 nsec are needed. The work in this paper presents a similar derivation of the bounds for different error distributions. Unlike the work presented here, [6] is focused on a limited set of scenarios and does not try to reveal the trend behavior by considering different network setup scenarios. Our previous work in [19] also outlines some of the issues presented in this paper, but does not consider angles at all. In contrast to [19], this paper presents the details of the bounds derivations, provides a more detailed evaluation over a larger set of network scenarios, and also includes a comparison of the error behavior for both distance and angle measurements. Furthermore, it provides the detailed CRB derivation for both cases and explores the trends in error propagation using carefully selected scenarios to account for the geometry effects.

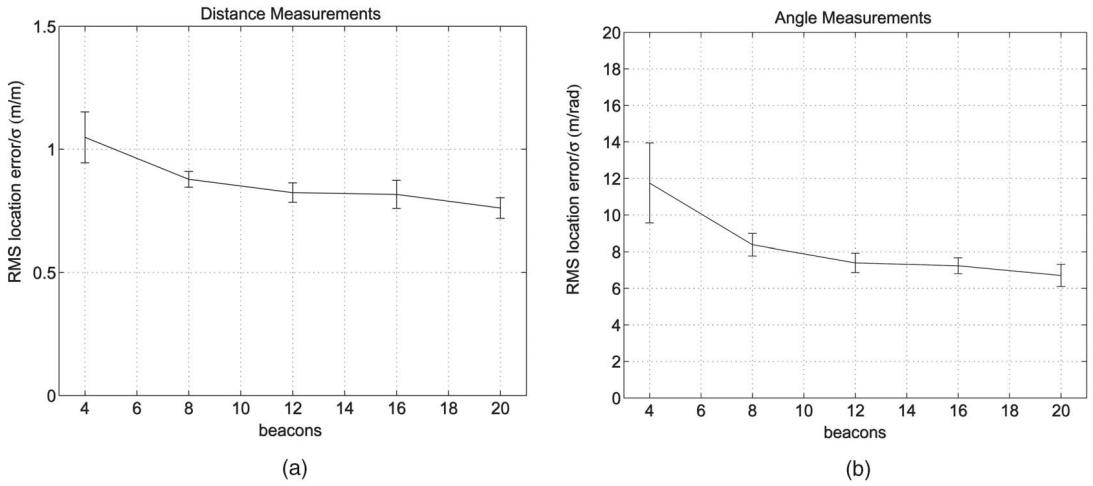

Fig. 7. Normalized RMS node localization error, (RMS error/σ) as a function of percentage of beacon nodes in the network. (a) Using distance-only measurements with distance measurement error $\sigma = \sigma_d$. (b) Using angle-only measurements with angle measurement error $\sigma = \sigma_\phi$.

6 Conclusions

In this paper, we have developed an analytical method for examining node location error in multihop networks. The analytical bounds developed here eliminate the need for expensive Monte-Carlo simulations. Moreover, the bounds help in developing and understanding the fundamentals of multihop node localization. In this paper, we applied the knowledge of the bounds to study the error trends with respect to network density, network scaling, percentage of beacons, and beacon uncertainty. Our simulation results have shown that location uncertainty decreased rapidly until 6-10 neighbors/node, then more gradually. Distance and angle measurements exhibit similar trends in localization error with varying network density. The error when angle-only measurements are used is much higher than when distance measurements are used. Furthermore, location error when angle-only measurements are used increased linearly with the distance between nodes. We also found that multihop localization is scalable since error propagation is very slow and since localization accuracy appears to be insensitive to increases in the number of beacon nodes. Finally, when the beacon uncertainty is high, most location error is an overall translation error of the entire network. Overall, we found that node localization can be more accurate when using distance measurements since the bounds predict that it is possible to obtain location estimates with lower uncertainty than the uncertainty in the distance measurement. The understanding of the error behavior with respect to the network setup parameters is also important in practical setups when evaluating localization systems. By applying this knowledge, one can determine which part of the error is due to setup parameters, thus helping to isolate and quantify algorithmic error and the error contribution due to changes in the surrounding environments.

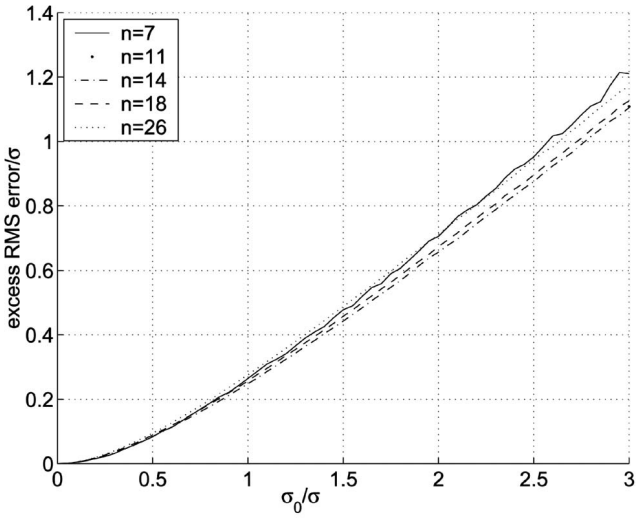

Fig. 8. Normalized RMS node localization error, (RMS error/σ) when beacon nodes have location uncertainty, as a function of normalized beacon uncertainty standard deviation (σ_0/σ). Localization error was computed using distance-only measurements. n denotes the number of neighbors per node.

References

[1] D. Niculescu and B. Nath, "Ad Hoc Positioning System (APS)," *Proc. IEEE GlobeCom,* pp. 2926-2931, Nov. 2001.
[2] D. Nicolescu and B. Nath, "Ad-Hoc Positioning System (APS) Using AOA," *Proc. IEEE INFOCOM,* 2003.
[3] C. Savarese, J. Rabay, and K. Langendoen, "Robust Positioning Algorithms for Distributed Ad-Hoc Wireless Sensor Networks," *Proc. USENIX Technical Ann. Conf.,* June 2002.
[4] A. Savvides, C.C. Han, and M.B. Srivastava, "Dynamic Fine-Grained Localization in Ad-Hoc Networks of Sensors," *Proc. Fifth Ann. Int'l Conf. Mobile Computing and Networking, Mobicom,* pp. 166-179, July 2001.
[5] A. Savvides, H. Park, and M.B. Srivistava, "The Bits and Flops of the N-Hop Multilateration Primitive for Node Localization Problems," *Proc. First ACM Int'l Workshop Wireless Sensor Networks and Applications (WSNA '02),* Sept. 2002.
[6] N. Patwari, A.O. Hero, M. Perkins, N.S. Correal, and R.J. O'Dea, "Relative Location Estimation in Wireless Sensor Networks," *IEEE Trans. Signal Processing,* Sept. 2003.
[7] R. Fontana and S. Gunderson, "Ultra Wideband Precision Asset Location System," *Proc. IEEE Conf. Ultra Wideband Systems and Technologies,* May 2002.
[8] http://www.bluesoft-inc.com, Bluesoft Inc., 2005.
[9] http://www.sick.de, SICK, 2005.
[10] R.L. Moses, D. Krishnamurthy, and R. Patterson, "A Self-Localization Method for Wireless Sensor Networks," *Eurasip J. Applied Signal Processing,* special issue on sensor networks, vol. 2003, pp. 348-353, Mar. 2003.

[11] A. Ihler, J.W. Fisher III, R.L. Moses, and A. Willsky, "Nonparametric Belief Propagation for Self-Calibration in Sensor Networks," *Proc. Third Int'l Symp. Information Processing in Sensor Networks (IPSN '04)*, 2004.
[12] H.L. Van Trees, *Detection, Estimation, and Modulation Theory: Part I.* New York: Wiley, 1968.
[13] M. Spirito, "On the Accuracy of Cellular Mobile Station Location Estimation," *IEEE Trans. Vehicular Technology*, vol. 50, no. 3, May 2001.
[14] D. Nicolescu and B. Nath, "Localized Positioning in Ad-Hoc Networks," *Elselvier J.*, special issue on ad hoc networks, May 2003.
[15] W.L. Garber, "Self-Localization of Sensor Networks," master's thesis, The Ohio State Univ., June 2003.
[16] R.L. Moses and R.M. Patterson, "Self-Calibration of Sensor Networks," *Unattended Ground Sensor Technologies and Applications IV (Proc. SPIE)*, vol. 4743, E.M. Carapezza, ed., pp. 108-119, Apr. 2002.
[17] K. Langendoen and N. Reijers, "Distributed Localization in Wireless Sensor Networks: A Quantitative Comparison," *Computer Networks*, special issue on wireless sensor networks, Aug. 2003.
[18] N. Patwari, R.J. O'Dea, and Y. Wang, "Relative Location in Wireless Networks," *Proc. IEEE Vehicular Technology Conf.*, vol. 2, pp. 1149-1153, May 2001.
[19] A. Savvides, W. Garber, S. Adlakha, R. Moses, and M.B. Srivastava, "On the Error Characteristics of Multihop Node Localization in Ad-Hoc Sensor Networks," *Proc. Information Processing in Sensor Networks Conf. (IPSN '03)*, Apr. 2003.

Andreas Savvides received the BS degree in electrical and computer engineering from the University of California, San Diego, in 1997, the MS degree in electrical engineering from the University of Massachusetts, Amherst, in 1999, and the PhD degree from the University of California, Los Angeles (UCLA) in 2003. During his graduate studies, Dr. Savvides was a member of the Center for Embedded Networked Sensing at UCLA. He is currently an assistant professor in the Electrical Engineering and Computer Science Departments at Yale University. He is the founder of the Embedded Networks and Applications Lab (ENALAB) and his research interests are in embedded systems, sensor networks, and smart environments. Dr. Savvides completed his undergraduate studies on a Fulbright Scholarship from 1993 to 1997, he received the Isenberg Award at the Isenberg School of Management at the University of Massachusetts Amherst in 1999, and received an award in the annual design competition at the IEEE Design Automation Conference in 2002.

Wendy L. Garber received the BS degree in electrical engineering (summa cum laude) from the University of Cincinnati, Cincinnati, Ohio, in 2001. She received the MS degree in electrical engineering from The Ohio State University, Columbus, Ohio, in 2003, supported by a US National Science Foundation Fellowship. She is currently with ATK Mission Research Corporation in Dayton, Ohio, where she works on advanced radar signal processing algorithms. She is a member of Eta Kapa Nu and Tau Beta Pi.

Randolph L. Moses (S'78-M'85-SM'90) received the BS, MS, and PhD degrees in electrical engineering from Virginia Polytechnic Institute and State University in 1979, 1980, and 1984, respectively. During the Summer of 1983, he was a SCEEE Summer Faculty Research Fellow at Rome Air Development Center, Rome, New York. From 1984 to 1985, he was with the Eindhoven University of Technology, Eindhoven, The Netherlands, as a NATO Postdoctoral Fellow. Since 1985, he has been with the Department of Electrical Engineering, The Ohio State University, and is currently a professor there. From 1994-1995, he was on sabbatical leave as a visiting researcher at the System and Control Group at Uppsala University in Sweden. His research interests are in digital signal processing, and include parametric time series analysis, radar signal processing, sensor array processing, and sensor networks. Dr. Moses was an associate editor for the *IEEE Transactions on Signal Processing* 2001-2004 and served on the technical committee on statistical signal and array processing of the IEEE Signal Processing Society from 1991-1994. He is coauthor with P. Stoica of *Introduction to Spectral Analysis* (Prentice Hall, 1997). He is a senior member of the IEEE and a member of Eta Kappa Nu, Tau Beta Pi, Phi Kappa Phi, and Sigma Xi.

Mani B. Srivastava received the BTech degree in electrical engineering from IIT Kanpur in 1985, and the MS and PhD degrees from the University of California at Berkeley in 1987 and 1992, respectively. He is currently a professor in the Electrical Engineering Department at the University of California, Los Angeles (UCLA). Prior to joining UCLA, he was a member of technical staff in the Networked Computing Research Department at Bell Laboratories from 1992 to 1996. His research interests at UCLA are in mobile and wireless networked embedded systems, focusing particularly on power-aware computing and communications, low-power design, sensor-instrumented physical spaces, wireless sensor networking, wireless QoS, and wireless node architectures. He has several patents in wireless systems, and has published extensively in the areas of wireless systems, sensor networks, and low-power embedded systems. He currently serves on the editorial boards of the *IEEE Transactions on Mobile Computing*, *ACM Mobile Computing and Communications Review*, and *Wiley's Wireless Communications and Mobile Computing*. He received the US National Science Foundation CAREER award in 1997, and the President of India Gold Medal in 1985. He is a senior member of the IEEE.